European Radiology (2020) 30:2182–2190
https://doi.org/10.1007/s00330-019-06574-1

NEURO

Wave-CAIPI susceptibility-weighted imaging achieves diagnostic performance comparable to conventional susceptibility-weighted imaging in half the scan time

Mi Sun Chung[1] · Eun Jung Lee[1] · Sujin Kim[1] · Seon-Ok Kim[2] · Jun Soo Byun[1]

Received: 11 March 2019 / Revised: 31 October 2019 / Accepted: 6 November 2019 / Published online: 17 January 2020

Abstract

Objectives We aimed to evaluate the agreement in the detection of cerebral microbleeds (CMBs) between conventional susceptibility-weighted imaging (SWI) and fast SWI using wave-controlled aliasing in parallel imaging (CAIPI) acceleration. We also scrutinized the diagnostic agreement for intracranial lesions and compared the image quality between both sequences.

Methods Institutional review board approval was obtained and informed consent was waived for this retrospective study. We included 181 consecutive patients who had undergone brain MRI with both conventional SWI (scan time, 251 s) and wave-CAIPI SWI (scan time, 113 s) from September 2017 to November 2017. All images were independently reviewed by two radiologists for the detection and counting of CMBs using the Microbleed Anatomical Rating Scale (MARS). One neuroradiologist diagnosed intracranial lesions and scored image quality using visual analysis. The agreement for detection of CMBs and intracranial lesions was calculated, and interobserver agreements were analyzed by using kappa and intraclass correlation.

Results For detection of CMBs, both the conventional and wave-CAIPI SWI showed significantly high agreement of 100% for the presence of CMBs, and 94.5% using MARS. Wave-CAIPI SWI achieved more than 97% agreement of MARS when divided by anatomical locations, with excellent agreement. Interobserver agreements were also excellent. The diagnosis for intracranial lesions (33 lesions in 28 patients) demonstrated 100% agreement. The image quality of both sequences is not significantly different ($p = 0.20$).

Conclusions Wave-CAIPI SWI achieved high agreement for CMB detection and diagnosis of intracranial lesions compared to conventional SWI within half of the scan time.

Key Points

- *Wave-CAIPI SWI achieves a diagnostic performance for the detection of cerebral microbleeds that is comparable to that of conventional SWI in half the scan time.*
- *Interobserver agreement for the detection (presence vs. absence) and counting of cerebral microbleeds of wave-CAIPI SWI was excellent.*
- *Wave-CAIPI SWI demonstrated a 100% agreement for the diagnosis of intracranial lesions and comparable image quality compared to conventional SWI.*

Keywords Magnetic resonance imaging · Brain · Hemorrhage · Diagnostic imaging

Abbreviations

CAIPIRINHA	Controlled aliasing in parallel imaging results in higher acceleration
CMBs	Cerebral microbleeds
GRAPPA	Generalized autocalibrating partially parallel acquisitions
ICC	Intraclass correlation
MARS	Microbleed Anatomical Rating Scale
SAR	Specific absorption rate
SENSE	Sensitivity encoding
SWI	Susceptibility-weighted imaging
TE	Echo time

Electronic supplementary material The online version of this article (https://doi.org/10.1007/s00330-019-06574-1) contains supplementary material, which is available to authorized users.

✉ Jun Soo Byun
flightdr61@hanmail.net

[1] Department of Radiology, Chung-Ang University Hospital, Chung-Ang University College of Medicine, 102 Heukseok-ro, Dongjak-gu, Seoul, Republic of Korea

[2] Department of Clinical Epidemiology and Biostatistics, Asan Medical Center, University of Ulsan College of Medicine, 86 Asanbyeongwon-Gil, Songpa-Gu, Seoul, Republic of Korea

Introduction

Cerebral microbleeds (CMBs) have been related to the normal aging process, medical treatments including oral contraceptives and antithrombotic agents, and various diseases such as traumatic brain injury, ischemic and hemorrhagic stroke, Alzheimer's disease, Parkinson's disease, and amyloid angiopathy [1–8]. Moreover, increased numbers of CMBs are associated with increased risk of vascular mortality, cognitive decline, and stroke [1, 2, 5, 6]. For the detection of CMBs, susceptibility-weighted imaging (SWI) allows the visualization of a greater number of CMBs than conventional gradient echo sequences [1, 9–11]. However, SWI requires more scan time and post-processing steps than conventional gradient echo imaging. The long scan time is the biggest obstacle, particularly in uncooperative patients with a higher probability of motion artifacts.

For the fast acquisition of SWI, parallel imaging techniques such as sensitivity encoding (SENSE), generalized autocalibrating partially parallel acquisitions (GRAPPA), and controlled aliasing in parallel imaging results in higher acceleration (CAIPIRINHA) have been extensively used to reduce the number of phase-encoding steps through the use of coil sensitivity encoding from multichannel receiver arrays [12–14]. Unfortunately, highly accelerated scans with known parallel acquisition techniques have some limitations for application in clinical practice, because whenever the parallel factor increases, image quality degrades due to noise amplification induced by the increased geometric (g) factor and the acquisition of fewer data points [15]. The wave-CAIPI technique has recently been proposed as a parallel imaging technique to obtain even greater parallel acceleration through the combination of the k-space undersampling technique of 2D-CAIPIRINHA and bunched phase encoding. "Wave-CAIPI" is named for the sinusoidal shape of its Gy and Gz gradients which are simultaneously varying during the frequency encoding step (with a $\pi/2$ phase shift between the two waveforms), and it creates a staggered corkscrew trajectory for k-space sampling [16, 17]. Wave-CAIPI has been suggested for fast 3D acquisition with low artifacts and negligible g-factor penalties for the acquisition of SWI, quantitative susceptibility mapping, rapid acquisition with refocusing echoes, and magnetization-prepared rapid gradient echo sequences [16–19]. To date, the usefulness of wave-CAIPI SWI compared to conventional SWI without wave-CAIPI acceleration has not been validated using patient data.

In this study, we aimed to evaluate the clinical feasibility of wave-CAIPI SWI for routine MRI scanning. We assessed the agreements for the detection of CMBs between conventional SWI and wave-CAIPI SWI. We also investigated the diagnostic agreement for intracranial lesions and compared image qualities in both sequences.

Materials and methods

Study population

We retrospectively included 181 consecutive patients who had undergone brain MRI with SWI from a single referral center from September 2017 to November 2017. The inclusion criteria were as follows: (1) patients who underwent brain MRI with SWI using both conventional and wave-CAIPI technique and (2) patient age > 20 years. Exclusion criteria were as follows: (1) MRI images with severe motion or metal artifacts and (2) data reconstruction failure. We retrospectively collected demographic and clinical data, including age, sex, history of head trauma, and past medical history of all the subjects by reviewing their electronic medical records.

Institutional review board approval was obtained and informed consent was waived for this retrospective study. We have reported the methods and results in accordance with the strengthening the reporting of observational studies in epidemiology (STROBE) guidelines [20].

Image acquisition

All MRIs were performed on two 3-T scanners (Magnetom Skyra, Siemens Healthineers) with 64 channel head coils under the IDEA environment. The detailed MR scan parameters of conventional and wave-CAIPI SWI are shown in Table 1. The total acquisition time was 251 s for conventional SWI and 113 s for wave-CAIPI SWI [21].

Table 1 Image parameters

	Conventional SWI	Wave-CAIPI SWI
Field of view (mm)	210 × 240	210 × 240
Voxel size (mm)	0.6 × 0.6 × 1.5	0.6 × 0.6 × 1.5
Matrix size	384 × 218	384 × 218
TR (ms)	28	40
TE (ms)	20	13.7/30.5 (mean TE, 22.1)
Band width (Hx/pixel)	120	120
Flip angle (°)	15	15
Parallel imaging method	GRAPPA	CAIPIRINHA
Acceleration factor (phase encoding direction)	2	2
Acceleration factor 3D (slice encoding direction)	–	3
Scan time (s)	251	113

CAIPIRINHA controlled aliasing in parallel imaging results in higher acceleration, *GRAPPA* generalized autocalibrating partially parallel acquisitions, *TE* echo time, *TR* repetition time

Image analysis

All MRIs were independently reviewed by two radiologists (M.S.C. and S.L.; 8 years and 14 years of experience, respectively) after a training session on the detection and counting of CMBs. The training session involved 10 cases of conventional and wave-CAIPI SWI from patients who had been excluded from the main analysis. Each observer performed image analysis independently, with a 2-week interval to prevent recall bias, and was blind to the results of the other observer and other sequences (conventional SWI or wave-CAIPI SWI).

The detection and counting of the CMBs were based on the Microbleed Anatomical Rating Scale (MARS) [22]. In this scale, CMBs are scored as "definite" or "possible"; we focused on definite CMBs. Definite CMBs in MARS are defined as small, rounded or circular, well-defined hypointense lesions within brain parenchyma, with clear margins ranging from 2 to 10 mm on SWI. The symmetrical areas of calcification in the basal ganglia, choroid plexus, and pineal gland signal intensity voids caused by sulcal vessels were excluded as well as low-signal intensity lesions including signal intensity voids due to adjacent bone structures [22–24]. For the scoring following MARS guidelines, observers counted the number of the CMBs in each location (brainstem, cerebellum, basal ganglia, thalamus, internal capsule, external capsule, corpus callosum, deep and periventricular white matter, frontal lobe, parietal lobe, temporal lobe, occipital lobe, and insula) and summed up the number of CMBs.

For the other intracranial lesions detected using SWI, one experienced neuroradiologist (M.S.C., 8 years of experience) performed diagnosis separately for each conventional and wave-CAIPI SWI, blind to the results of other sequences (conventional SWI or wave-CAIPI SWI). When other intracranial lesions besides CMB were suspected on conventional or wave-CAIPI SWI, T2-weighted imaging, fluid-attenuated inversion recovery (FLAIR), or diffusion weighted imaging were used to confirm the diagnosis [22]. We also diagnosed cerebral amyloid angiopathy using Boston criteria [25, 26] and hypertensive arteriopathy using the distribution of CMBs (CMBs located in both basal ganglia, thalami, and brainstem).

The overall image quality and motion artifact of both conventional and wave-CAIPI SWI were scored by using a five-level scale based on visual analysis: 1 = nondiagnostic image quality featuring strong artifacts; 2 = severe blurring rendering evaluation uncertain; 3 = moderate blurring that slightly compromises assessment; 4 = slight blurring that did not compromise image assessment; and 5 = excellent image quality without artifacts. For the susceptibility artifact, the visibility of basilar artery and artifacts in both temporal lobes are visually evaluated. The visibility of the basilar artery was graded by using a five-level scale as follows: 1 = no visualization of the vessel due to susceptibility artifact; 2 = severe artifact allowing only detection of the location of the vessel; 3 = moderate artifact causing limitation of evaluation in the arterial stenosis; 4 = slight blurring that did not compromise image assessment; and 5 = excellent image without artifacts. The artifacts in both temporal lobes were graded using the same method assessing overall image quality.

Statistical analysis

Statistical analyses were performed by a statistician (S.K.). The summary statistics are presented as the number and percentages for categorical variables, and the means with standard deviations for continuous variables. The agreement for the presence of CMBs and MARS in the entire brain between conventional and wave-CAIPI SWI was calculated as follows: number of the patients that agree/total number of patients × 100 (%). The two-sided 95% confidence interval of the agreements was estimated using the Wilson score method. We also performed additional analysis for the agreement of the number of CMBs classified by location following the anatomical classification of MARS using intraclass correlation (ICC).

The interobserver agreement for the presence of CMBs and MARS on conventional and wave-CAIPI SWI in whole brain and each anatomical location was analyzed using the kappa value and ICC. The image qualities were compared by using the Wilcoxon signed rank test.

The kappa results were interpreted as being in poor (0–0.20), fair (0.21–0.40), moderate (0.41–0.60), good (0.61–0.80), or very good (0.81–1) agreement [27]. An ICC of less than 0.40 was considered as poor; 0.40 to 0.59 as fair; 0.60 to 0.74 as good; and 0.75 to 1.00 as excellent [28]. All statistical analyses were performed using MedCalc, version 15.0 (MedCalc Software), or SPSS software (version 20.0; SPSS).

Results

The mean age of the study population was 60.5 ± 16.7 years (range, 20–87 years; male to female ratio [n] = 82:99). The mean specific absorption rate (SAR) for wave-CAIPI SWI is significantly larger than conventional SWI (mean ± standard deviation, 0.044 ± 0.005 for wave-CAIPI vs. 0.016 ± 0.002 for conventional SWI, $p < 0.001$).

Agreement for the detection of CMBs between conventional and wave-CAIPI SWI

For the detection of CMBs, the conventional and wave-CAIPI SWI demonstrated 100% of agreement in the pooled analysis

Table 2 The detection of CMBs between conventional and wave-CAIPI SWI

	Conventional SWI	Wave-CAIPI SWI	Agreement (*n* of agreement/total, 95% CI)	Kappa value/ICC (95% CI)
Presence of CMBs[†]				
Overall	35.6% (129/362)	35.6% (129/362)	100% (362/362, 98.0–100.00)	1.00
Observer 1	35.4% (64/181)	35.4% (64/181)	100% (181/181, 98.0–100.00)	1.00
Observer 2	35.9% (65/181)	35.9% (65/181)	100% (181/181, 98.0–100.00)	1.00
MARS[††]				
Overall	1.1 ± 2.7 (0–22)	1.1 ± 2.6 (0–20)	94.5% (342/362, 90.1–97.3)	0.997 (0.996–0.998)
Observer 1	1.0 ± 2.6 (0–21)	1.0 ± 2.4 (0–18)	96.7% (175/181, 92.9–98.8)	0.989 (0.985–0.992)
Observer 2	1.2 ± 2.8 (0–22)	1.2 ± 2.8 (0–20)	95.0% (172/181, 90.8–97.7)	0.995 (0.993–0.996)

CMBs cerebral microbleeds, *CI* confidence interval, *ICC* intraclass correlation, *MARS* Microbleed Anatomical Rating Scale

[†] Presence of cerebral microbleeds is calculated by the number of the patients with cerebral microbleed/total number of patients

[††] MARS for conventional SWI and wave-CAIPI SWI were presented with mean ± standard deviation (range)

and for each observer (Table 2 and Fig. 1). For the exact number of CMBs using the MARS, the conventional and wave-CAIPI SWI also showed a high agreement of 94.5% (Table 2). Wave-CAIPI SWI also achieved more than 97% agreement of MARS score in all anatomical locations of brain parenchyma, with excellent agreement (Supplemental Table 1 and 2).

Interobserver agreement for the detection of CMBs

Interobserver agreement for the presence and number of CMBs following MARS was excellent in both conventional and wave-CAIPI SWI (Table 3). Wave-CAIPI SWI demonstrated a 99.5% agreement for the presence of CMBs and 88.4% for the number of CMBs. Moreover, all anatomical locations except the right parietal lobe and temporal lobe demonstrated more than good agreement (Supplemental Table 3). In the right parietal lobe and temporal lobe, wave-CAIPI SWI demonstrated relatively lower ICC in comparison with conventional SWI.

Diagnostic performance of intracranial lesions

Thirty-three lesions from 28 patients were diagnosed using both conventional and wave-CAIPI SWI. The diagnosis for intracranial lesions using both conventional and wave-CAIPI SWI demonstrated 100% agreement. The diagnosis included 10 acute or subacute hemorrhages (Fig. 2), 5 infarctions with hemorrhagic transformation (Fig. 3), 13 old hemorrhage sequelae (3 superficial siderosis and 10 encephalomalatic

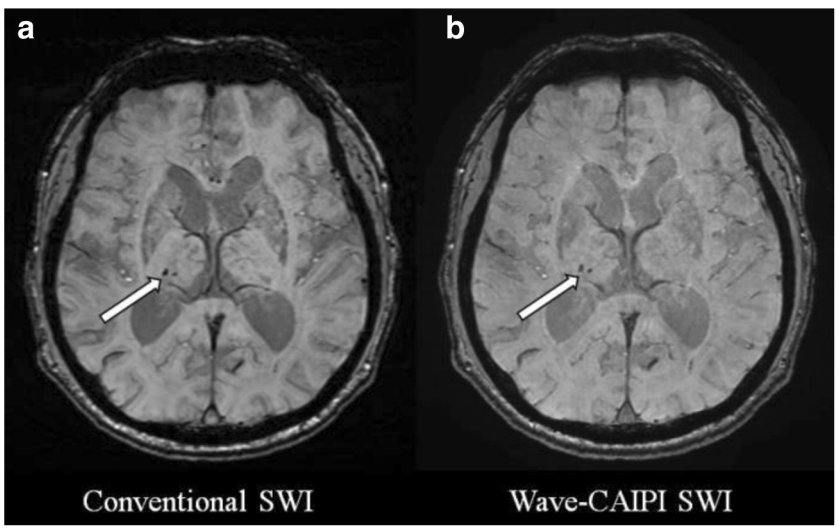

Fig. 1 Detection of CMBs using conventional and wave-CAIPI SWI. Two CMBs (arrow) in the right thalamus are visualized well in both conventional (**a**) and wave-CAIPI SWI (**b**). CMBs, cerebral microbleeds

Table 3 Interobserver agreement of detection of CMBs on conventional and wave-CAIPI SWI

	Agreement (n of agreement/total, 95% CI)	Kappa value/ICC (95% CI)
Presence of CMBs		
Overall	99.5% (360/362, 97.0–100.0)	0.988 (0.964–1.000)
Conventional SWI	99.5% (180/181, 97.0–100.0)	0.988 (0.964–1.000)
Wave-CAIPI SWI	99.5% (180/181, 97.0–100.0)	0.988 (0.964–1.000)
MARS		
Overall	87.9% (318/362, 82.2–92.2)	0.979 (0.972–0.984)
Conventional SWI	90.1% (163/181, 84.7–94.0)	0.965 (0.954–0.974)
Wave-CAIPI SWI	88.4% (160/181, 82.8–92.7)	0.947 (0.929–0.960)

CMBs cerebral microbleeds, *CI* confidence interval, *ICC* intraclass correlation, *MARS* Microbleed Anatomical Rating Scale

changes with old hemorrhage), 4 developmental venous anomalies (Fig. 4), and 1 parenchymal calcification. Furthermore, 5 patients with hypertensive arteriopathy and 7 patients with cerebral amyloid angiopathy were diagnosed considering distribution of CMBs and show 100% diagnostic agreement between two sequences.

Image qualities of wave-CAIPI SWI

The image quality scores of conventional and wave-CAIPI SWI were comparable (median [interquartile range], 5 [5–5] for conventional SWI vs. 5 [4–5] for wave-CAIPI SWI, $p = 0.20$). The motion artifact of conventional and wave-CAIPI SWI had no difference (5 [5–5] for conventional SWI vs. 5 [5–5] for wave-CAIPI SWI, $p = 0.10$). The susceptibility artifact of wave-CAIPI SWI was less for the visualization of the basilar artery (3 [2–5] for conventional SWI vs. 4 [4–5] for wave-CAIPI SWI, $p < 0.001$, Fig. 5) compared with conventional SWI. Furthermore, susceptibility artifacts in the temporal lobes are less prominent in wave-CAIPI SWI (5 [5–5] for conventional SWI vs. 5 [5–5] for wave-CAIPI SWI, $p < 0.001$, Fig. 5) compared to those of conventional SWI.

Discussion

In this study, we demonstrated that wave-CAIPI SWI is a feasible and reliable fast SWI method for the detection and counting of CMBs compared to conventional SWI without wave-CAIPI acceleration; scan time could be reduced by approximately 50% when using wave-CAIPI SWI. Moreover, with wave-CAIPI SWI, the diagnosis of intracranial lesions, including hemorrhages and hemorrhagic transformation after strokes, shows 100% agreement with conventional SWI. The

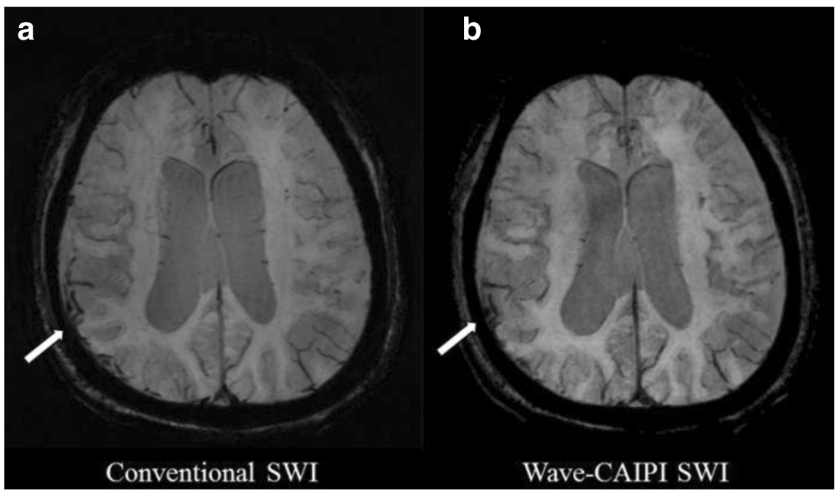

Fig. 2 Hemorrhage on conventional and wave-CAIPI SWI. A scanty amount of subarachnoid hemorrhage (arrow) in the right temporal convexity is diagnosed using both conventional (**a**) and wave-CAIPI SWI (**b**)

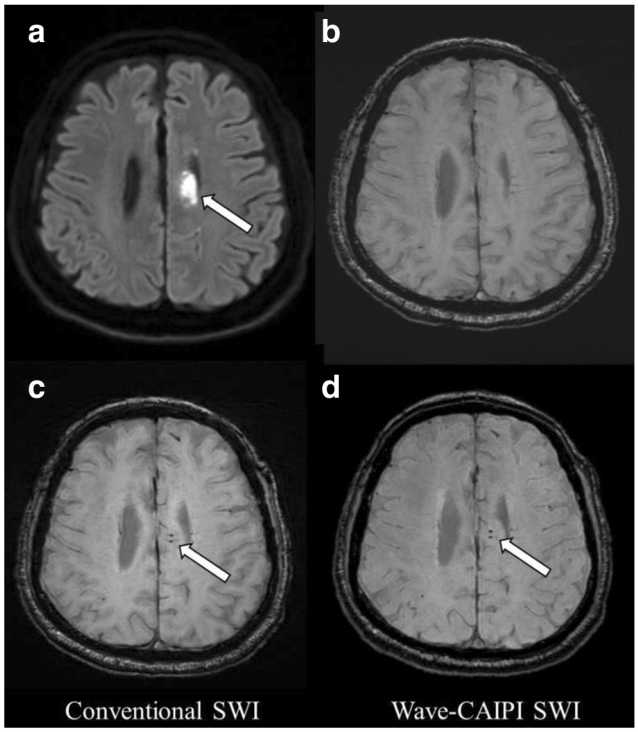

Fig. 3 Early hemorrhagic transformation on conventional and wave-CAIPI SWI. A 70-year-old male who had acute infarction (arrowhead) in the left anterior cerebral artery territory in the diffusion weighted image (**a**) did not have any CMBs in the infarct area in the initial conventional SWI (**b**). However, newly developing CMBs (arrow), which suggest petechial hemorrhage caused by early-stage hemorrhagic transformation, are detected upon 4-day follow-up imaging (**c** and **d**). Both conventional SWI (**c**) and wave-CAIPI SWI (**d**) demonstrate early hemorrhagic transformation in the infarct area well. CMB, cerebral microbleeds

image qualities of conventional and wave-CAIPI SWI are comparable. Thus, we suggested that fast SWI, based on wave-CAIPI, could be an alternative for conventional SWI in daily practice. The wave-CAIPI technique-based fast SWI could be beneficial to the widespread application of SWI, especially in uncooperative patients with higher probabilities of motion artifacts.

Controlling aliasing is a key issue toward the realization of faster MRI with a high acceleration factor because increased g-factor from the summation of aliased voxels induces noise amplification in images with high parallel acquisition [16, 29]. Wave-CAIPI encoding plays sinusoidal gradients during the readout to achieve a corkscrew trajectory in k-space and cause voxel spreading effect in frequency encoding direction [17, 21]. The center of each corkscrew is arranged in a staggered pattern according to 2D-CAIPIRINHA sampling scheme (slice and phase encoding direction) [16, 17, 21]. The combined effect of 2D-CAIPIRINHA and corkscrew k-space trajectory of wave-encoding can result in a highly efficient k-space sampling pattern and simultaneously maximize the distance between aliased voxels evenly in all spatial dimensions (x, y, and z) [16, 17, 21, 29]. In addition, wave-CAIPI traverses k-space in a line-by-line manner with constant velocity along the frequency encoding direction; it has less undesirable image distortion/blurring artifacts from magnetic field strength variations. In the setting of the relatively lower bandwidth readout (e.g., 100–400 Hz/pixel) of structural imaging, the wave-CAIPI technique could be more effective because larger corkscrew trajectories can be used for the effective spreading of voxel aliasing compared to a higher bandwidth [29]. For the SWI, wave-CAIPI SWI designed to be flow-compensated and used dual echo time (TE) with the mean TE corresponds to the desired TE to increase signal-to-noise ratio [21]. The reconstructed multiecho data were combined through root sum of square for the magnitude and TE-weighted combination of the unwrapped echo phases to generate wave-CAIPI SWI images [21].

We also note an interesting feature regarding less prominent susceptibility artifacts of wave-CAIPI SWI in the air-bone interface resulting in better visualization of the basilar artery and both temporal lobes. The possible reason for the decreased prominence of susceptibility artifacts is the use of dual TE of wave-CAIPI SWI (first TE, 13.7 ms; second TE, 30.5 ms). The first TE of wave-CAIPI SWI is shorter than the TE of conventional SWI (20 ms). This shorter first TE contributes to the reduction of susceptibility artifacts by allowing less time for spin dephasing and increased the signal-to-noise ratio [30, 31]. Even though the mean TE of wave-CAIPI SWI is similar to the TE of conventional SWI, the shorter first TE of wave-CAIPI SWI could contribute to the decreased susceptibility artifacts in the air-bone interface. Less prominent susceptibility artifacts could have some advantage for the evaluation of patients with vascular pathology in the basilar and vertebral arteries (e.g., dissection or intraluminal thrombus) and in patients with larger sinuses or metallic devices. However, we also observed less susceptibility of wave-CAIPI SWI which caused slight blurring in the contour of vascular lesions such as developmental venous anomalies (Fig. 4), even though diagnostic accuracy did not decrease. A previous study, which applied multigradient-echo images for the reduction of susceptibility-induced signal loss, demonstrated that macroscopic susceptibility artifacts caused by the tissue-air interface in the orbital frontal cortex and temporal lobe are decreased in shorter TE images compared with longer TE images [32]. They reconstructed images from different TEs using weighting factors to minimize signal loss and better signal-to-noise ratio (long TEs for improved signal-to-noise ratio in the brain area free from major macroscopic field inhomogeneity and short TEs in the area affected by field inhomogeneities such as orbitofrontal cortexes). For wave-CAIPI SWI, applying short TE would be helpful to depict lesions inside severe macroscopic susceptibility artifacts. Simultaneously, it might slightly decrease mesoscopic or microscopic susceptibilities, although this property does not ruin the diagnostic performance of wave-CAIPI SWI. Therefore, further clinical validations and investigations for the

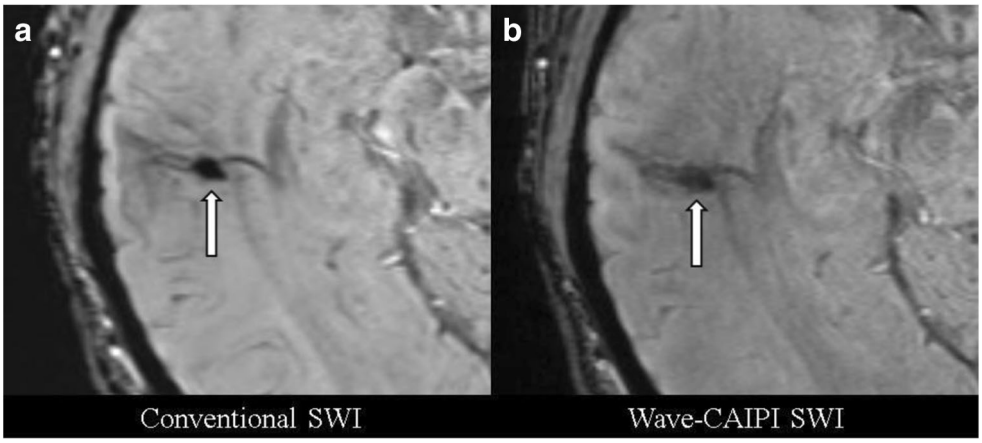

Fig. 4 Developmental venous anomaly on conventional and wave-CAIPI SWI. A 42-year-old male who had dizziness underwent an MRI for evaluation. Both conventional SWI (**a**) and wave-CAIPI SWI (**b**) are well-visualized; the collection of dilated medullary veins converging in an enlarged subependymal collector vein in the right temporal lobe suggests a classical umbrella-shaped pattern of the developmental venous anomaly. However, the margins of the developmental venous anomaly are slightly blurred in wave-CAIPI SWI compared to that in conventional SWI, even though detection of the focal lesion is not affected by the decreased image quality

susceptibility effect and optimization of scan parameters for wave-CAIPI SWI are warranted.

Simultaneously, wave-CAIPI SWI could have several drawbacks in clinical applications. First, compared with conventional SWI, wave-CAIPI SWI has higher levels of SAR and it might be caused by dual echo time of wave-CAIPI SWI. However, SWI based on the gradient echo images requires smaller radiofrequencies to generate small flip angles compared to spin echo images [33, 34]. Therefore, increased SAR from wave-CAIPI techniques is not a main contributor of SAR hazard; wave-CAIPI SWI demonstrated only 10% of SAR in a turbo spin echo T2-weighted image in our institution. Second, previous technical research suggested the possibility of worsened motion artifacts in images using the wave-CAIPI technique [17]. On the other hand, motion artifacts were comparable between two sequences in this study. We speculated that shorter scan time of wave-CAIPI SWI had a decreased chance to encounter patient motions during MRI scanning. The actual clinical implication of wave-CAIPI sequences toward patients with higher probability of motion artifacts seems to need further clinical validations. Third, wave-CAIPI SWI needs more computational power for image reconstruction from fewer data points, and a well-designed multichannel coil system could take full advantage of the higher acceleration of wave-CAIPI sequences.

There were also several limitations to note in this study. First, selection bias could be introduced because this study was

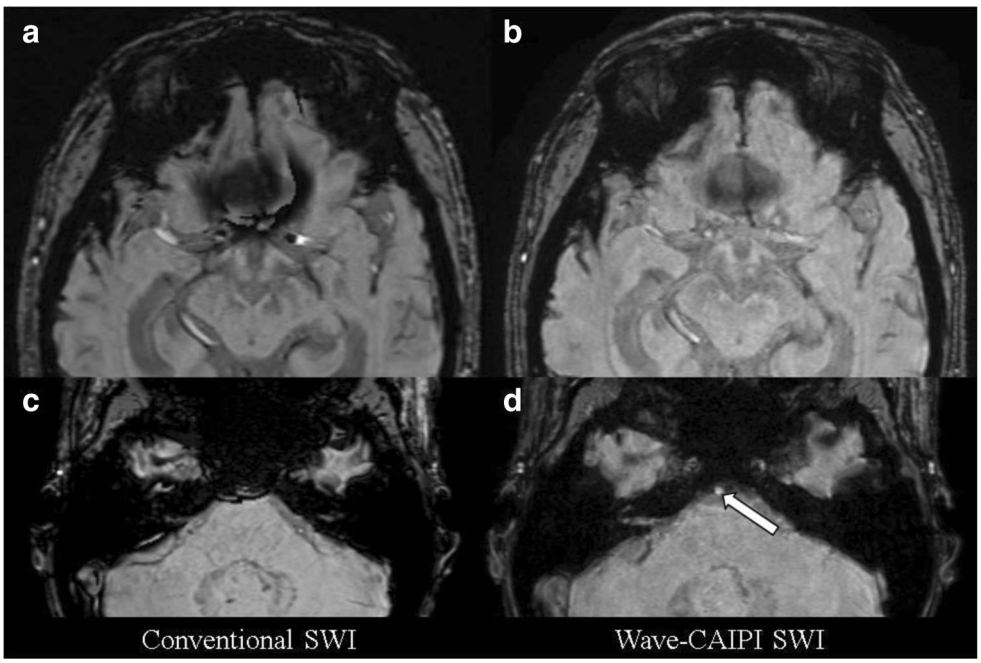

Fig. 5 Susceptibility artifacts on conventional and wave-CAIPI SWI. Both orbitofrontal cortices on conventional SWI are poorly visualized due to a large extent of susceptibility artifacts caused by both ethmoid sinuses (**a**). The extents of the artifacts are decreased on wave-CAIPI SWI (**b**). The basilar artery is hardly visible on conventional SWI due to susceptibility artifacts caused by sphenoid sinus on conventional SWI (**c**). However, the patient's basilar artery (arrow) is detected when using wave-CAIPI SWI (**d**). The areas in both temporal lobes which are obscured by susceptibility artifacts from mastoid air cells and sphenoid sinuses are also less obscured on wave-CAIPI SWI (**d**) compared to conventional SWI (**c**)

performed at a single referral center. In this study, we proved the high diagnostic performance of wave-CAIPI SWI for the detection of CMBs and various kinds of intracranial diseases. Based on our results, further multicenter studies will be needed to validate generalized applications of wave-CAIPI sequences. Second, we focused on diagnostic performance for the detection and counting of CMBs with fast SWI using wave-CAIPI. Therefore, limited numbers of patients with intracranial lesions were included, and the clinical implications of the use of wave-CAIPI SWI for patients with specific diseases (such as hemorrhage or acute stroke) were not fully evaluated in this study.

In conclusion, wave-CAIPI SWI is a reliable method for the detection and counting of CMBs within approximately half of the scan time of conventional SWI without the wave-CAIPI technique. For the diagnosis of intracranial lesions, wave-CAIPI SWI demonstrated 100% agreement with conventional SWI, and the image qualities of wave-CAIPI SWI and conventional SWI are comparable. Considering reduced scan time with preservation of diagnostic performance, wave-CAIPI SWI could be an alternative for conventional SWI in daily practice.

Acknowledgments The wave-CAIPI sequence was obtained from Dr. Kawin Setsompop and Dr. Stephen Cauley at the A.A. Martinos Center, through the Siemens C2P sharing program. In Seong Kim at Siemens Healthineers Korea helped to install and optimize scan parameters of wave-CAIPI SWI.

Funding information The authors state that this work has not received any funding.

Compliance with ethical standards

Guarantor The scientific guarantor of this publication is Prof. Byung Ihn Choi.

Conflict of interest The authors declare that they have no competing interests.

Statistics and biometry One of the authors (S.K.) has significant statistical expertise.

Informed consent Written informed consent was waived by the Institutional Review Board.

Ethical approval Institutional Review Board approval was obtained.

Methodology
- retrospective
- observational
- performed at one institution

References

1. Kim BJ, Lee S-H (2013) Cerebral microbleeds: their associated factors, radiologic findings, and clinical implications. J Stroke 15: 153–163
2. Akoudad S, Portegies ML, Koudstaal PJ et al (2015) Cerebral microbleeds are associated with an increased risk of stroke: the Rotterdam Study. Circulation 132:509–516
3. Ding J, Sigurdsson S, Garcia M et al (2015) Risk factors associated with incident cerebral microbleeds according to location in older people: the Age, Gene/Environment Susceptibility (AGES)-Reykjavik Study. JAMA Neurol 72:682–688
4. Del Brutto VJ, Zambrano M, Mera RM, Del Brutto OH (2015) Population-based study of cerebral microbleeds in stroke-free older adults living in rural Ecuador: the Atahualpa Project. Stroke 46: 1984–1986
5. Miwa K, Tanaka M, Okazaki S et al (2014) Multiple or mixed cerebral microbleeds and dementia in patients with vascular risk factors. Neurology 83:646–653
6. Nagasawa J, Kiyozaka T, Ikeda K (2014) Prevalence and clinicoradiological analyses of patients with Alzheimer disease coexisting multiple microbleeds. J Stroke Cerebrovasc Dis 23: 2444–2449
7. Shams S, Martola J, Granberg T et al (2015) Cerebral microbleeds: different prevalence, topography, and risk factors depending on dementia diagnosis-the Karolinska Imaging Dementia Study. AJNR Am J Neuroradiol 36:661–666
8. Romero JR, Preis SR, Beiser A et al (2014) Risk factors, stroke prevention treatments, and prevalence of cerebral microbleeds in the Framingham Heart Study. Stroke 45:1492–1494
9. Goos JDC, van der Flier WM, Knol DL et al (2011) Clinical relevance of improved microbleed detection by susceptibility-weighted magnetic resonance imaging. Stroke 42:1894–1900
10. Guo L, Wang G, Zhu X, Liu C, Cui L (2013) Comparison of ESWAN, SWI-SPGR, and 2D T2*-weighted GRE sequence for depicting cerebral microbleeds. Clin Neuroradiol 23:121–127
11. Cheng A-L, Batool S, McCreary CR et al (2013) Susceptibility-weighted imaging is more reliable than T2*-weighted gradient-recalled Echo MRI for detecting microbleeds. Stroke 44:2782–2786
12. Pruessmann KP, Weiger M, Scheidegger MB, Boesiger P (1999) SENSE: sensitivity encoding for fast MRI. Magn Reson Med 42: 952–962
13. Griswold MA, Jakob PM, Heidemann RM et al (2002) Generalized autocalibrating partially parallel acquisitions (GRAPPA). Magn Reson Med 47:1202–1210
14. Breuer FA, Blaimer M, Heidemann RM, Mueller MF, Griswold MA, Jakob PM (2005) Controlled aliasing in parallel imaging results in higher acceleration (CAIPIRINHA) for multi-slice imaging. Magn Reson Med 53:684–691
15. Robson PM, Grant AK, Madhuranthakam AJ, Lattanzi R, Sodickson DK, McKenzie CA (2008) Comprehensive quantification of signal-to-noise ratio and g-factor for image-based and k-space-based parallel imaging reconstructions. Magn Reson Med 60:895–907
16. Bilgic B, Xie L, Dibb R et al (2016) Rapid multi-orientation quantitative susceptibility mapping. Neuroimage 125:1131–1141
17. Bilgic B, Gagoski BA, Cauley SF et al (2015) Wave-CAIPI for highly accelerated 3D imaging. Magn Reson Med 73:2152–2162
18. Polak D, Setsompop K, Cauley SF et al (2018) Wave-CAIPI for highly accelerated MP-RAGE imaging. Magn Reson Med 79:401–406
19. Gagoski BA, Bilgic B, Eichner C et al (2015) RARE/turbo spin echo imaging with simultaneous multislice wave-CAIPI. Magn Reson Med 73:929–938
20. von Elm E, Altman DG, Egger M, Pocock SJ, Gotzsche PC, Vandenbroucke JP (2007) Strengthening the Reporting of Observational Studies in Epidemiology (STROBE) statement: guidelines for reporting observational studies. BMJ 335:806–808
21. Cauley SF, Setsompop K, Bilgic B, Bhat H, Gagoski B, Wald LL (2017) Autocalibrated wave-CAIPI reconstruction; joint

optimization of k-space trajectory and parallel imaging reconstruction. Magn Reson Med 78:1093–1099
22. Gregoire S, Chaudhary U, Brown M et al (2009) The microbleed anatomical rating scale (MARS) reliability of a tool to map brain microbleeds. Neurology 73:1759–1766
23. Greenberg SM, Vernooij MW, Cordonnier C et al (2009) Cerebral microbleeds: a guide to detection and interpretation. Lancet Neurol 8:165–174
24. Jeerakathil T, Wolf PA, Beiser A et al (2004) Cerebral microbleeds: prevalence and associations with cardiovascular risk factors in the Framingham Study. Stroke 35:1831–1835
25. Linn J, Halpin A, Demaerel P et al (2010) Prevalence of superficial siderosis in patients with cerebral amyloid angiopathy. Neurology 74:1346–1350
26. Greenberg Steven M, Charidimou A (2018) Diagnosis of cerebral amyloid angiopathy. Stroke 49:491–497
27. Landis JR, Koch GG (1977) The measurement of observer agreement for categorical data. Biometrics 33:159–174
28. Shrout PE, Fleiss JL (1979) Intraclass correlations: uses in assessing rater reliability. Psychol Bull 86:420–428
29. Setsompop K, Feinberg DA, Polimeni JR (2016) Rapid brain MRI acquisition techniques at ultra-high fields. NMR Biomed 29:1198–1221
30. Huang SY, Seethamraju RT, Patel P, Hahn PF, Kirsch JE, Guimaraes AR (2015) Body MR imaging: artifacts, k-space, and solutions-erratum. Radiographics 35:1624
31. Gorno-Tempini ML, Hutton C, Josephs O, Deichmann R, Price C, Turner R (2002) Echo time dependence of BOLD contrast and susceptibility artifacts. Neuroimage 15:136–142
32. Volz S, Hattingen E, Preibisch C, Gasser T, Deichmann R (2009) Reduction of susceptibility-induced signal losses in multi-gradient-echo images: application to improved visualization of the subthalamic nucleus. Neuroimage 45:1135–1143
33. Allison J, Yanasak N (2015) What MRI sequences produce the highest specific absorption rate (SAR), and is there something we should be doing to reduce the SAR during standard examinations? AJR Am J Roentgenol 205:W140–W140
34. Boss A, Graf H, Berger A et al (2007) Tissue warming and regulatory responses induced by radio frequency energy deposition on a whole-body 3-tesla magnetic resonance imager. J Magn Reson Imaging 26:1334–1339